Characteristic Analysis of An Ironless Linear Synchronous Motor with Novel Halbach Magnet Array

Lu Zhang, Baoquan Kou, Feng Xing, and Binchao Zhao

Department of Electrical Engineering, Harbin Institute of Technology, Harbin, 150001 China

Abstract—A novel ironless synchronous permanent magnet linear motor with Halbach array is proposed. The operation principle and structure of this linear motor are introduced. Based on magnetic vector potential equation and boundary conditions, flux density distribution induced by the permanent magnet array is analysed analytically. And then the expression of the air-gap flux density distribution was derived. Characteristics such as thrust and back-EMF are obtained analytically and compared with the finite element simulation results. A prototype machine is manufactured and some experimental study is carried out, which validate the analytical and simulated results.

I. Introduction

At present, there exist many various applications with linear motor in all parts of the industry. In some special applications, the low torque ripple and high precision position control are needed. In this case, the permanent magnet linear synchronous motor with moving ironless windings seems to be as suitable electrical machine[1-7]. In this paper, an ironless permanent magnet linear synchronous motor (ILPMLSM) with a novel double side Halbach array is analysed, as shown in Fig. 1. The ILPMLSM consists of a novel double side Halbach permanent magnet array and an air core type moving coils which are concentrated winding having three isolated phase sets.

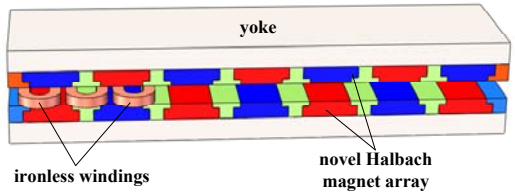

Fig. 1. The novel ILPMLSM proposed in this paper.

II. Air-gap Flux Density

It is necessary to gain the air-gap flux density of the ILPMLSM, because the dynamic performance and the precision of the ILPMLSM is greatly influenced by the distribution of the magnetic field that generated by the novel double side Halbach permanent magnet array. Recently, many numerical methods have been proposed to analyse motor's performance through field analysis. As one of the numerical methods, the finite element method (FEM) allows an accurate analysis of electrical machines and can consider geometric details and the non-linearity of magnetic material [5]. However, it is time consuming and unsuitable for the initial design stages and optimization from dynamic analysis. Therefore, an analytical method, which is to solve the Poisson equation is usually used for magnetic field analysis because of their fast and flexible computation [7-9].

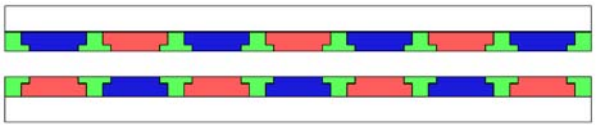

Fig. 2. The novel double side Halbach permanent magnet array.

The novel double side Halbach permanent magnet array that proposed in this paper is shown in Fig.2. Since the double side permanent magnet linear motor has a symmetric structure along y-axis, only one side is selected as the analysis region.[10,11]

The magnetic field of the novel Halbach permanent magnets is approximated with the analytical solution of the magnetic field of an ideal permanent magnet. And some assumptions are made in order to simplify the model, such as: all regions are extended infinitely in the *x* direction, permanent magnets are periodically distributed along the x-axis, the permeability of the yoke is infinite and the permeability of the permanent magnet material is equal to the permeability of free space[12-15].

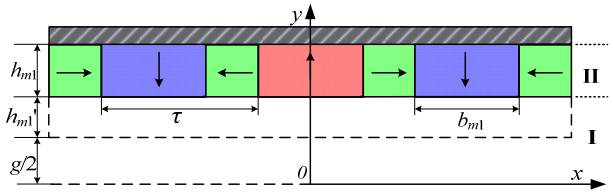

(a) the top-part

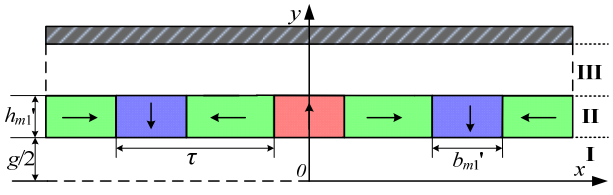

(b) the bottom-part

Fig. 3. Analytical model of the ILPMLSM.

In Fig.3, the analytical model of the one side Halbach

permanent magnet array is divided into two parts, the top-part and the bottom-part. Based on the equivalent magnetization intensity method, the air-gap flux density distribution of the motor will be obtained by calculating the vector sum of the field generated by all the magnets in the novel double side Halbach array[16].

In Fig.3 (a), the model is divided into two regions. In region I and II, the magnetic vector potential satisfies the Poisson equation (1) and boundary conditions (2).

$$\begin{cases} \dfrac{\partial^2 \vec{A}_{\mathrm{zI}}}{\partial x^2}+\dfrac{\partial^2 \vec{A}_{\mathrm{zI}}}{\partial y^2}=0 \\ \dfrac{\partial^2 \vec{A}_{\mathrm{zII}}}{\partial x^2}+\dfrac{\partial^2 \vec{A}_{\mathrm{zII}}}{\partial y^2}=-\mu_0 \vec{J}_{\mathrm{M}} \end{cases} \tag{1}$$

where A_z is the z-axis component of the vector magnetic potential, J_M is equivalent magnetizing current density.

$$\begin{cases} H_{\mathrm{xI}}\big|_{y=0}=0 \\ B_{\mathrm{yI}}\big|_{y=\frac{g}{2}+h_{\mathrm{m1}}'}=B_{\mathrm{yII}}\big|_{y=\frac{g}{2}+h_{\mathrm{m1}}'} \\ H_{\mathrm{xII}}\big|_{y=\frac{g}{2}+h_{\mathrm{m1}}'}-H_{\mathrm{xI}}\big|_{y=\frac{g}{2}+h_{\mathrm{m1}}'}=M_{\mathrm{x}} \\ H_{\mathrm{xII}}\big|_{y=\frac{g}{2}+h_{\mathrm{m1}}'+h_{\mathrm{m1}}}=M_{\mathrm{x}} \end{cases} \tag{2}$$

According to the boundary conditions, Variable Separation Method is used to solve the governing equation, taking into account of the permanent magnet array periodicity and symmetry over the x, the normal components B_y of the flux density produced by the PMs of the top-part of the air gap can be written as

$$\begin{aligned} B_{\mathrm{yI}}=-\sum_{n=1}^{\infty}\Bigg\{ & \frac{K_n-\left\{K_n\cosh\left[m_n\left(\frac{g}{2}+h_{\mathrm{m1}}'\right)\right]+T_n\sinh\left[m_n\left(\frac{g}{2}+h_{\mathrm{m1}}'\right)\right]\right\}}{\sinh\left[m_n\left(\frac{g}{2}+h_{\mathrm{m1}}'+h_{\mathrm{m1}}\right)\right]} \\ & \cdot\cosh\left[m_n\left(\frac{g}{2}+h_{\mathrm{m1}}'+h_{\mathrm{m1}}\right)\right]+K_n\sinh\left[m_n\left(\frac{g}{2}+h_{\mathrm{m1}}'\right)\right] \\ & +T_n\cosh\left[m_n\left(\frac{g}{2}+h_{\mathrm{m1}}'\right)\right]\Bigg\}m_n\cosh(m_n y)\cos(m_n x) \end{aligned} \tag{3}$$

where m_n= (2n-1) π/τ,

$$T_n=(-1)\frac{4B_{\mathrm{r}}}{\tau m_n^2}\sin\frac{(2n-1)\pi\alpha_{\mathrm{p}}}{2};\ K_n=\frac{4B_{\mathrm{r}}}{\tau m_n^2}\cos\frac{(2n-1)\pi\alpha_{\mathrm{p}}}{2}$$

In Fig.3 (b), the vector magnetic potential satisfies the Poisson equation (4) and boundary conditions (5) similar.

$$\begin{cases} \dfrac{\partial^2 \vec{A}_{\mathrm{zI}}'}{\partial x^2}+\dfrac{\partial^2 \vec{A}_{\mathrm{zI}}'}{\partial y^2}=0 \\ \dfrac{\partial^2 \vec{A}_{\mathrm{zII}}'}{\partial x^2}+\dfrac{\partial^2 \vec{A}_{\mathrm{zII}}'}{\partial y^2}=-\mu_0 \vec{J}_{\mathrm{M}}' \\ \dfrac{\partial^2 \vec{A}_{\mathrm{zIII}}'}{\partial x^2}+\dfrac{\partial^2 \vec{A}_{\mathrm{zIII}}'}{\partial y^2}=0 \end{cases} \tag{4}$$

$$\begin{cases} H_{\mathrm{xI}}'\big|_{y=0}=0 \\ B_{\mathrm{yI}}'\big|_{y=\frac{g}{2}}=B_{\mathrm{yII}}'\big|_{y=\frac{g}{2}} \\ H_{\mathrm{xII}}'\big|_{y=\frac{g}{2}}-H_{\mathrm{xI}}'\big|_{y=\frac{g}{2}}=M_{\mathrm{x}}' \\ B_{\mathrm{yII}}'\big|_{y=\frac{g}{2}+h_{\mathrm{m1}}'}=B_{\mathrm{yIII}}'\big|_{y=\frac{g}{2}+h_{\mathrm{m1}}'} \\ H_{\mathrm{xII}}'\big|_{y=\frac{g}{2}+h_{\mathrm{m1}}'}-H_{\mathrm{xIII}}'\big|_{y=\frac{g}{2}+h_{\mathrm{m1}}'}=M_{\mathrm{x}}' \\ H_{\mathrm{xIII}}'\big|_{y=\frac{g}{2}+h_{\mathrm{m1}}'+h_{\mathrm{m1}}}=0 \end{cases} \tag{5}$$

By applying the boundary conditions to the interfaces between different material regions, the solution of governing equations (7) can be obtained. The normal components B_y of the flux density produced by the PMs of the bottom-part of the air gap is provided from the curl of A_z and is given as follows

$$\begin{aligned} B_{\mathrm{yI}}'=\sum_{n=1}^{\infty}\Bigg\{ & \Bigg\{\frac{K_n'\left\{\cosh\left(m_n\frac{g}{2}\right)-\cosh\left[m_n\left(\frac{g}{2}+h_{\mathrm{m1}}'\right)\right]\right\}}{-\sinh\left[m_n\left(\frac{g}{2}+h_{\mathrm{m1}}'+h_{\mathrm{m1}}\right)\right]} \\ & +\frac{T_n'\left\{\sinh\left(m_n\frac{g}{2}\right)-\sinh\left[m_n\left(\frac{g}{2}+h_{\mathrm{m1}}'\right)\right]\right\}}{-\sinh\left[m_n\left(\frac{g}{2}+h_{\mathrm{m1}}'+h_{\mathrm{m1}}\right)\right]}\Bigg\} \\ & \cdot\cosh\left[m_n\left(\frac{g}{2}+h_{\mathrm{m1}}'+h_{\mathrm{m1}}\right)\right] \\ & +K_n'\left\{\sinh\left(m_n\frac{g}{2}\right)-\sinh\left[m_n\left(\frac{g}{2}+h_{\mathrm{m1}}'\right)\right]\right\} \\ & +T_n'\left\{\cosh\left(m_n\frac{g}{2}\right)-\cosh\left[m_n\left(\frac{g}{2}+h_{\mathrm{m1}}'\right)\right]\right\}\Bigg\} \\ & \cdot m_n\cosh(m_n y)\cos(m_n x) \end{aligned} \tag{6}$$

The whole B_y in the air-gap now is obtained by superposition

of the magnetic field that induced by the top-part and the bottom-part. The reasonableness of the analytical method is validated by finite element method, as shown in Fig. 4.

$$B_y = B_{y1} + B'_{y1} \tag{7}$$

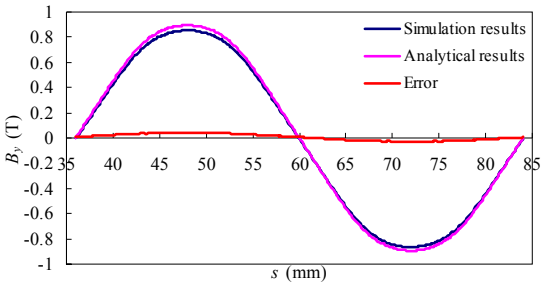

Fig. 4. Comparison of B_y between the analytical method and FEM.

III. Characteristic Analysis of the ILPMLSM

A. The Back Electromotive Force

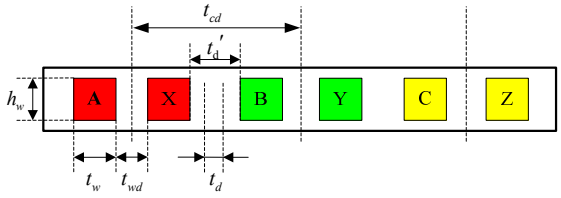

Fig. 5. The cross-section distribution of the winding.

Fig. 5 shows the cross-section distribution of the winding of the ILPMLSM. The ironless winding is a concentrated winding and have three isolated phase sets. Three phase coils are displaced symmetrically at every 120° circumferentially and the current waveform in the phases is a 120° sine wave. Assuming the ironless windings moving with a velocity v_s, the expression of the back-EMF of coils A-X with N turns can be also derived as follows

$$\begin{aligned} E_{ax} &= e_A - e_X \\ &= Nl_w v_s (B_{avA} - B_{avX}) \\ &= Nl_w v_s \left[\frac{\int_{x+t_d/2}^{x+t_d/2+t_w} \int_{-h_w/2}^{h_w/2} B_{ym} \cosh(m_n y)\cos(m_n x)\mathrm{d}y\mathrm{d}x}{t_w h_w} \right. \\ &\quad \left. - \frac{\int_{x+t_d/2+t_w+t_{wd}}^{x+t_d/2+2t_w+t_{wd}} \int_{-h_w/2}^{h_w/2} B_{ym} \cosh(m_n y)\cos(m_n x)\mathrm{d}y\mathrm{d}x}{t_w h_w} \right] \\ &= \frac{8NB_{ym} l_w v_s}{t_w h_w m_n^2} \sinh\left(m_n \frac{h_w}{2}\right) \sin\left(m_n \frac{t_w}{2}\right) \\ &\quad \cdot \sin\left(m_n \frac{t_{cd} - t_w - t_d}{2}\right) \sin\left[m_n \left(x + \frac{t_{cd}}{2}\right)\right] \end{aligned} \tag{8}$$

where B_{ym} is the amplitude of the B_y.

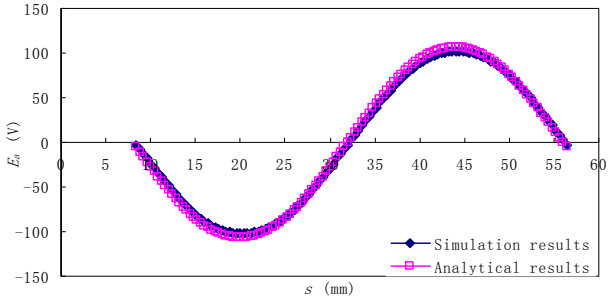

Fig. 6. Comparison of E_a between the analytical method and FEM.

From Fig. 6 it can be observed that the analytical results coincide with the simulation results well, and the max error is only about 4.06%[16].

B. The Electromagnetic Force

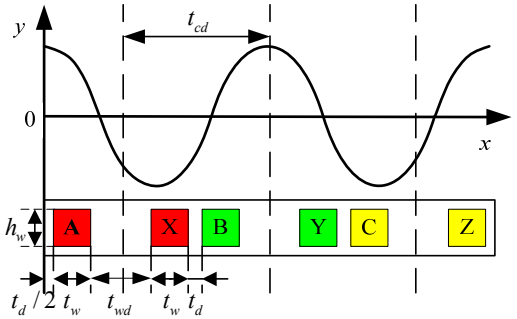

Fig. 7. The model used to derive the electronic thrust.

Fig. 7 shows the model used for deriving the electronic thrust. And in Fig. 7, the current density function of winding A can be written as

$$J_a(x) = \begin{cases} J_{a0}, & \frac{t_d}{2} \le x \le \frac{t_d}{2} + t_w \\ -J_{a0}, & \frac{t_d}{2} + t_w + t_{wd} \le x \le \frac{t_d}{2} + 2t_w + t_{wd} \\ 0, & 0 < x < \frac{t_d}{2} \,\&\, \frac{t_d}{2} + t_w < x < \frac{t_d}{2} + t_w + t_{wd} \,\& \\ & \frac{t_d}{2} + 2t_w + t_{wd} < x < t_{cd} \end{cases} \tag{9}$$

where $J_{a0}=\sqrt{2}\,NI\sin(\theta_0)/(h_w \cdot t_w)$, θ_0 is the initial angle, N is the turns of the coil.

According to the Lorentz force law, the force on a current carrying conductor in a magnetic field can be expressed as

$$\vec{F} = \int_V \vec{J} \times \vec{B} dV \tag{10}$$

Then, the electronic thrust of the winding A of the novel ironless permanent magnet linear synchronous motor is derived as follows

$$
\begin{aligned}
F_{\mathrm{A}} &= \int_0^{\frac{4}{3}\tau}\int_{-h_{\mathrm{w}}/2}^{h_{\mathrm{w}}/2} B_{\mathrm{ym}}\cosh(m_n y)\cos(m_n x) l_{\mathrm{w}} J_{\mathrm{a}}(x)\mathrm{d}y\mathrm{d}x \\
&= \frac{2B_{\mathrm{ym}} l_{\mathrm{w}}\sinh(m_n\frac{h_{\mathrm{w}}}{2})}{m_n}\left[\int_{\frac{t_{\mathrm{d}}}{2}}^{\frac{t_{\mathrm{d}}}{2}+t_{\mathrm{w}}} J_{\mathrm{a0}}\cos(m_n x)\mathrm{d}x - \int_{\frac{t_{\mathrm{d}}}{2}+t_{\mathrm{w}}+t_{\mathrm{wd}}}^{\frac{t_{\mathrm{d}}}{2}+2t_{\mathrm{w}}+t_{\mathrm{wd}}} J_{\mathrm{a0}}\cos(m_n x)\mathrm{d}x\right] \\
&= \frac{2B_{\mathrm{ym}} l_{\mathrm{w}} J_{\mathrm{a0}}\sinh(m_n\frac{h_{\mathrm{w}}}{2})}{m_n^2}\left\{\sin[m_n(\frac{t_{\mathrm{d}}}{2}+t_{\mathrm{w}})]-\sin(m_n\frac{t_{\mathrm{d}}}{2})\right. \\
&\quad \left.-\sin[m_n(\frac{t_{\mathrm{d}}}{2}+2t_{\mathrm{w}}+t_{\mathrm{wd}})]+\sin[m_n(\frac{t_{\mathrm{d}}}{2}+t_{\mathrm{w}}+t_{\mathrm{wd}})]\right\}
\end{aligned} \tag{11}
$$

Similarly, the current density function of winding B and C can be written as (12) and (13).

$$
J_{\mathrm{b}}(x)=\begin{cases}
J_{\mathrm{b0}}\ , & \frac{t_{\mathrm{d}}}{2}+t_{\mathrm{cd}}\le x\le\frac{t_{\mathrm{d}}}{2}+t_{\mathrm{w}}+t_{\mathrm{cd}} \\
-J_{\mathrm{b0}}\ , & \frac{t_{\mathrm{d}}}{2}+t_{\mathrm{w}}+t_{\mathrm{wd}}+t_{\mathrm{cd}}\le x\le\frac{t_{\mathrm{d}}}{2}+2t_{\mathrm{w}}+t_{\mathrm{wd}}+t_{\mathrm{cd}} \\
0\ , & t_{\mathrm{cd}}<x<\frac{t_{\mathrm{d}}}{2}+t_{\mathrm{cd}}\ \&\ \frac{t_{\mathrm{d}}}{2}+t_{\mathrm{w}}+t_{\mathrm{cd}}<x<\frac{t_{\mathrm{d}}}{2}+t_{\mathrm{w}}+t_{\mathrm{wd}}+t_{\mathrm{cd}}\ \& \\
 & \frac{t_{\mathrm{d}}}{2}+2t_{\mathrm{w}}+t_{\mathrm{wd}}+t_{\mathrm{cd}}<x<2t_{\mathrm{cd}}
\end{cases} \tag{12}
$$

$$
J_{\mathrm{c}}(x)=\begin{cases}
J_{\mathrm{c0}}\ , & \frac{t_{\mathrm{d}}}{2}+2t_{\mathrm{cd}}\le x\le\frac{t_{\mathrm{d}}}{2}+t_{\mathrm{w}}+2t_{\mathrm{cd}} \\
-J_{\mathrm{c0}}\ , & \frac{t_{\mathrm{d}}}{2}+t_{\mathrm{w}}+t_{\mathrm{wd}}+2t_{\mathrm{cd}}\le x\le\frac{t_{\mathrm{d}}}{2}+2t_{\mathrm{w}}+t_{\mathrm{wd}}+2t_{\mathrm{cd}} \\
0\ , & 2t_{\mathrm{cd}}<x<\frac{t_{\mathrm{d}}}{2}+2t_{\mathrm{cd}}\ \&\ \frac{t_{\mathrm{d}}}{2}+t_{\mathrm{w}}+2t_{\mathrm{cd}}<x<\frac{t_{\mathrm{d}}}{2}+t_{\mathrm{w}}+t_{\mathrm{wd}}+2t_{\mathrm{cd}}\ \& \\
 & \frac{t_{\mathrm{d}}}{2}+2t_{\mathrm{w}}+t_{\mathrm{wd}}+2t_{\mathrm{cd}}<x<3t_{\mathrm{cd}}
\end{cases} \tag{13}
$$

The electronic thrust of the winding B and C can be derived according to the Lorentz force law also, and the expressions are shown as (14) and (15).

$$
\begin{aligned}
F_{\mathrm{B}} &= \frac{2B_{\mathrm{ym}} l_{\mathrm{w}} J_{\mathrm{b0}}\sinh(m_n\frac{h_{\mathrm{w}}}{2})}{m_n^2}\left\{\sin[m_n(\frac{t_{\mathrm{d}}}{2}+t_{\mathrm{w}}+t_{\mathrm{cd}})]-\sin\left[m_n(\frac{t_{\mathrm{d}}}{2}+t_{\mathrm{cd}})\right]\right. \\
&\quad \left.-\sin[m_n(\frac{t_{\mathrm{d}}}{2}+2t_{\mathrm{w}}+t_{\mathrm{wd}}+t_{\mathrm{cd}})]+\sin[m_n(\frac{t_{\mathrm{d}}}{2}+t_{\mathrm{w}}+t_{\mathrm{wd}}+t_{\mathrm{cd}})]\right\}
\end{aligned} \tag{14}
$$

$$
\begin{aligned}
F_{\mathrm{C}} &= \frac{2B_{\mathrm{ym}} l_{\mathrm{w}} J_{\mathrm{c0}}\sinh(m_n\frac{h_{\mathrm{w}}}{2})}{m_n^2}\left\{\sin[m_n(\frac{t_{\mathrm{d}}}{2}+t_{\mathrm{w}}+2t_{\mathrm{cd}})]-\sin\left[m_n(\frac{t_{\mathrm{d}}}{2}+2t_{\mathrm{cd}})\right]\right. \\
&\quad \left.-\sin[m_n(\frac{t_{\mathrm{d}}}{2}+2t_{\mathrm{w}}+t_{\mathrm{wd}}+2t_{\mathrm{cd}})]+\sin[m_n(\frac{t_{\mathrm{d}}}{2}+t_{\mathrm{w}}+t_{\mathrm{wd}}+2t_{\mathrm{cd}})]\right\}
\end{aligned} \tag{15}
$$

The total electronic thrust of the novel ironless permanent magnet linear synchronous motor is

$$
F = F_{\mathrm{A}} + F_{\mathrm{B}} + F_{\mathrm{C}} \tag{16}
$$

Fig. 8 shows the comparison of F between the analytical method and FEM. The average value of the electronic thrust that obtained by the analytical method is about 283.7N, and the average value of the electronic thrust that obtained by the FEM is about 272.4N. The results that obtained from the two methods are basically the same and the error is about 4.15%[16].

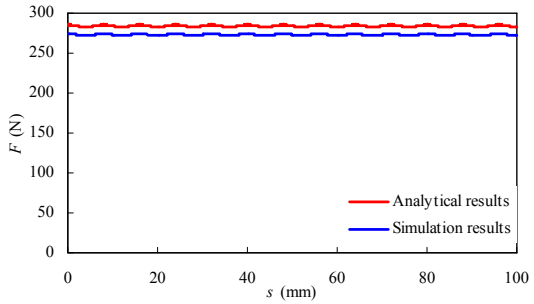

Fig. 8. Comparison of F between the analytical method and FEM.

IV. Prototype and Experiment

A prototype motor is manufactured in laboratories based on the previous analysis, as shown in Fig. 9. Table I shows the specification data of the ILPMLSM.

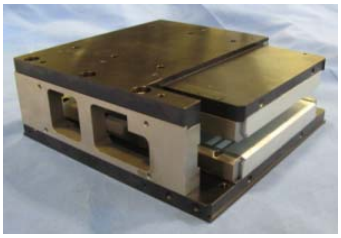

(a) the stator

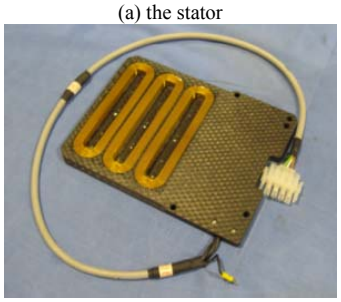

(b) the mover

Fig. 9. The prototype of the ILPMLSM.

TABLE I
Dimensions of the Motor

Part	Item	Symbol	Value	Unit
Mover	pitch of the coil	t_{cd}	32	mm
	coil cross-section width	t_w	7.9	mm
	coil cross-section height	h_w	8.4	mm
	distance between two coils	t_d	2.8	mm
Air-gap	length	g	11	mm
Stator	pitch of the magnet	τ	24	mm
	thickness	h_m	12	mm

Fig. 10 shows the test platform of the ILPMLSM and some experiments are carried out with the prototype. The experimental results are validated by the finite-element method. The no-load back-EMF of the three phase windings is measured, while the mover is moved in the x-direction with a constant speed v_x=0.05m/s. The measured results are shown in Fig.11, and the waveform is well sinusoid.

Fig. 10. The test platform of the ILPMLSM.

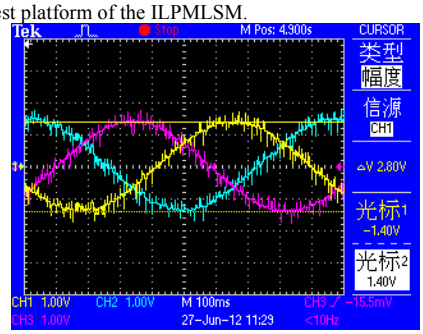

Fig. 11. The no-load back-EMF waveform.

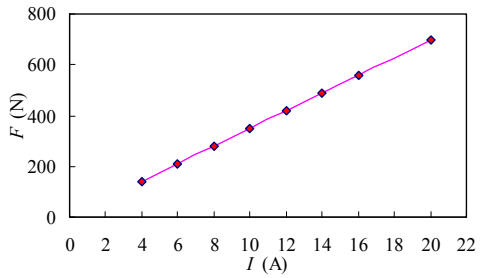

Fig. 12. The curve of the thrust with current RMS.

To verify the linearity of the thrust of the ILPMLSM, the input current of one phase was changed and the static thrust was measured. Fig. 12 shows the curves of maximum thrust versus input current. It can be found that the trend of the curves is basically linear.

V. Conclusions

In this paper, we proposed an ironless permanent magnet linear synchronous motor with a novel double side Halbach array. The flux density that produced by the novel double side Halbach array was solved analytically by solving the vector magnetic potential equations. The expressions of the air-gap flux density in the *y*-direction has been acquired. Characteristics such as the back electromotive force and the electromagnetic force were investigated analytically and validated by FEM. A prototype has been manufactured, and it's reasonable was validated by experiments.

Acknowledgment

This work was supported by the National Science and Technology Major Project (2009ZX02207-001).

References

[1] Kim W J, Berhan M T, Trumper D L, et al, "Analysis and implementation of a tubular motor with Halbach magnet array," *Industry Applications Conference*, 1996: 471-478.

[2] Jang S M, Jeong S S, Cha S D, "The application of linear Halbach array to eddy current rail brake system," *IEEE Transactions on Magnetics*, Vol. 37, No. 4, pp. 2627-2629, 2001.

[3] A. H. Isfahani, S. Vaez-Zadeh, "Design optimization of a linear permanent magnet synchronous motor for extra low force pulsations," *Energy Conversion and Management*, Vol. 48, No. 2, pp. 443-449, 2007.

[4] Z. Q. Zhu, and D. Howe, "Halbach permanent magnet machines and applications: A review," *IEE Proceeding of Electric Power Applications*, Vol. 148, No. 4, pp. 299-308, July 2001.

[5] Jang S, Sung, L, "Comparison of two types of PM linear synchronous servo and miniature motor with air cored film coil," *IEEE Transactions on Magnetics*, Vol. 38, No. 5, pp. 3264–3266, 2002.

[6] Ham C H, Ko W, "Development of a maglev propulsion system based on the Halbach magnet arrays," *IEEE International Magnetics Conference*, 2006.

[7] Li H F, Xia C L, "Halbach array magnet and its application to PM spherical motor," *International Conference on Electrical Machines and Systems*, 2008: 3064-3069.

[8] Mizuno T, Yamada H, "Magnetic circuit analysis of a linear synchronous motor with permanent magnet," *IEEE Transactions on Magnetics*, Vol. 28, No. 5, pp. 3027–3029, 1992.

[9] Sun P, Zhou H X, "Air-gap magnetic field design optimization for U-shaped ironless permanent magnet linear synchronous motors," *International Conference on Electrical Machines and Systems*, 2008, pp. 358-363.

[10] Zhang Q, Pan M C, Chen D X, "Analytic calculation of magnetic field and force in Halbach permanent magnet linear motor," *The Tenth International Conference on Electronic Measurement & Instruments*, 2011: 77-80.

[11] G. Zhou, X. L. Huang, H. Jiang, L. Tan, and J. N. Dong, "Analysis method to a Halbach PM ironless linear motor with trapezoid windings," *IEEE Transactions on Magnetics*, Vol. 47, No. 10, pp. 4167-4170, October 2011.

[12] Ferkova Z, Franko M, Kucht J, Rafajdus P, "Electromagnetic design of ironless permanent magnet synchronous linear motor," *International Symposium on Power Electronics, Electrical Drives, Automation and Motion*, 2008: 721-726.

[13] Trumper D L, Kim W J, Williams M E, "Design and analysis framework for linear permanent-magnet machines," *IEEE Transactions on Industry Applications*, Vol. 32, No. 4, pp. 371–379, 1996.

[14] A. H. Isfahani, S. Vaez-Zadeh, "Multi objective design optimization of air-core linear permanent magnet synchronous motors for improved thrust and low magnet consumption," *IEEE Transactions on Magnetics*. Vol. 42, No. 3, pp. 445-452, 2006.

[15] Nariman R T, Abbas S, "Minimizing thrust fluctuation in linear permanent magnet synchronous motor with Halbach array," *1st Power Electronic & Drive Systems & Technologies Conference*, 2010: 302-306.

[16] Zhao Binchao, "Research on ironless permanent magnet linear synchronous motor with Halbach secondary structure," Harbin: Harbin Institute of Technology, 2012(in Chinese).